ISSUE: June 2023

Designing An Open-Source Power Inverter (Part 13): The Differential Boost Push-Pull Power-Transfer Circuit

by Dennis Feucht, Innovatia Laboratories, Cayo, Belize

Early on in this series,[1-12] we described the reasoning behind the overall power architecture and the choice of circuits used in the three power stages of the Volksinverter (Fig. 1). For instance, in part 3 we discussed three different options for the power transfer circuit used in the battery converter (dc-dc) stage.[3] We considered push-pull (PP), boost push-pull (BPP) and SEPIC topologies, ultimately concluding that boost push-pull was the optimum of the three. We did further analysis in part 11 to compare the BPP circuit with both PP and single-ended PWM-switch circuits to determine which scheme yielded lower switching losses, with the BPP coming out ahead again.[11]

However, there is another variation on the BPP that deserves consideration. This part introduces a circuit modification of the common-active (CA) PWM-switch or boost push-pull (BPP) power-transfer circuit that changes it to an interleaved or *differential BPP* (DBPP)—differential in circuit symmetry. We'll also compare the BPP and the DBPP power transfer circuits. In the next part in the series, the DBPP will be compared to a bridge-switched common-passive or buck (CP-BRG) transfer circuit to determine whether a boost push-pull (CA-PP) or CP-BRG has lower loss as a low-R_g power-transfer circuit.

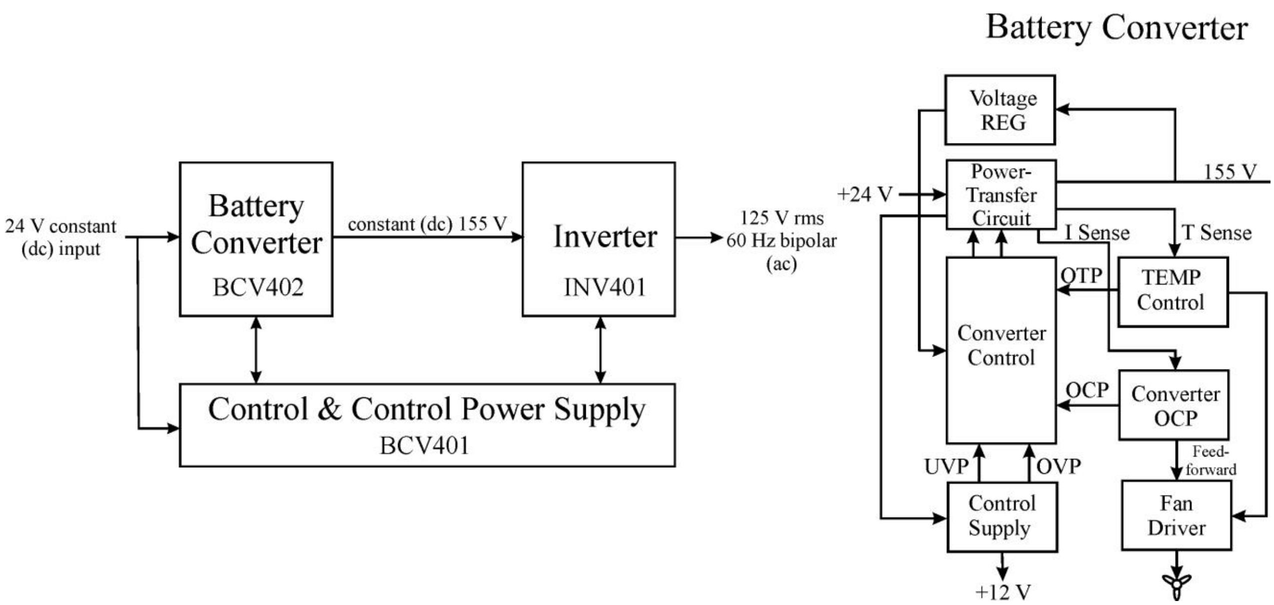

Fig. 1. The Volksinverter's system block diagram (left) and the BCV402 battery converter stage block diagram (right). In previous parts of this series, it's been determined that the boost push-pull is the optimum topology for the power transfer circuit. But in this part 13 we revisit that decision by considering a variation on the BPP known as the differential boost push-pull or DBPP.

CA-PP (BPP) Power-Transfer Circuit

As noted above, a decision was made favoring the common-active push-pull (CA-PP) or boost push-pull (BPP) circuit of Fig. 2. Its switch loss was shown to be lower than the alternatives of a push-pull chopper or unipolar PWM-switch transfer circuits including Ćuk-switch circuits.[11]

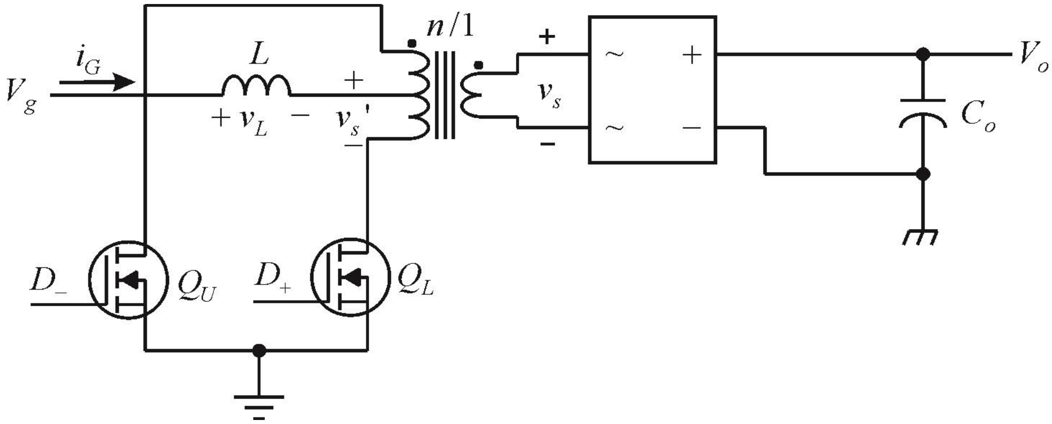

Fig. 2. The CA (boost) push-pull power-transfer circuit (BPP) with low switch and winding form-factor products. The center-tapped primary winding is regarded as two identical but oppositely-phased primary windings. Each winding has a turns ratio of $n = N_p/N_s$. The MOSFET power switches are driven with duty-ratios D_+ and D_- .

The interleaved or *differential* BPP (DBPP) is a BPP modification that combines the two BPP primary windings in series, leaving a single primary winding and adding a second input inductor, as shown in Fig. 3. The original BPP inductor is split into two smaller inductors of half the current rating. Although this adds one more magnetic component, construction is simplified because for a low-R_g (input resistance) converter the large wire size is reduced and is easier to wind on a toroid core. The two smaller inductors do not add much more space than the single BPP inductor.

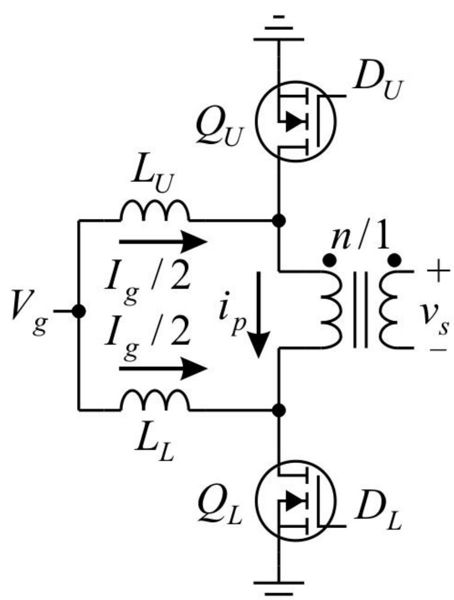

Fig. 3. The interleaved or differential boost push-pull (DBPP) primary circuit. A BPP primary winding is traded for an extra inductor. The switch formulas are the same but the primary winding current waveforms are different.

The DBPP switch sequencing is that of the BPP. Power is transferred from primary to secondary winding during off-time as in any CA (boost) circuit. For the same transfer power at half the primary current, the secondary-referred off-time voltage across the primary winding must be twice that of the BPP primary windings.

The DBPP has the same off-switch voltage as the BPP and the same switch voltage rating. Furthermore, the primary winding is now fully utilized as is switch voltage. In every switching cycle (or magnetic half-cycle), the primary winding conducts inductor current during off-time, transferring power to the secondary winding.

In the magnetic design, the primary winding is reduced somewhat in size from the BPP optimum of 60% of the winding window to 50% of the winding window for the DBPP. With the same turns as the BPP primary windings in series and wire size of half the BPP ampacity, transformer size is reduced somewhat for the same transfer power because primary winding utilization is doubled; the full DBPP primary winding is used to transfer power each cycle whereas in the BPP, the two windings alternate each cycle in transferring power.

The DBPP primary winding effectively has an on-time transfer resistance increase of ×4 over the BPP; comparing with BPP V_s' and I_g, $R_{pDBPP} = 2 \cdot V_s'/(I_g/2) = 4 \cdot R_{pBPP}$. Only the transformer primary winding, not the DBPP switches, have less loss than the BPP. The switches have the same voltage and current ratings and the same current waveforms.

The DBPP primary winding is equivalent to both BPP primary windings in series, but the DBPP winding transfers power on both magnetic half-cycles whereas only half of the BPP primary windings transfers each cycle. Thus, DBPP primary winding utilization $U_p = 1$. In both BPP and DBPP circuits, the secondary winding drives a full-wave (FW) rectifier for full secondary winding utilization. Consequently, the transformer for the DBPP, like that of the CP-BRG (common-passive, full bridge) circuit, has overall utilization $U = 1$. The DBPP waveforms are shown in Fig. 4.

Average ($\bar{i}$) and RMS ($\tilde{i}$) currents of the ports, switches, and windings assume transformer magnetizing current $i_{mp} << i_p$ and $i_m \approx 0$ A (the small-ripple approximation) which leads us to the following expressions for average and RMS currents, and switch form factors:

$$\bar{i}_g = I_g \; ; \; \bar{i}_L = I_g/2 \; ; \; \tilde{i}_g \approx \bar{i}_g$$

$$\bar{i}_Q = D \cdot \left(\frac{I_g}{2}\right) + \tfrac{1}{2} \cdot D' \cdot I_g = \frac{I_g}{2} \; ; \; \tilde{i}_Q = \sqrt{D \cdot \left(\frac{I_g}{2}\right)^2 + \frac{D'}{2} \cdot I_g^2} = \frac{I_g}{2} \cdot \sqrt{1 + D'}$$

$$|\bar{i}_p| = \frac{I_g}{2} \cdot D' \; ; \; |\bar{i}_s(\mathrm{FW})| = D' \cdot I_s = D' \cdot n \cdot I_p \; ; \; \bar{i}_D = \tfrac{1}{2} \cdot |\bar{i}_s(\mathrm{FW})|$$

$$\tilde{i}_p = \frac{I_g}{2} \cdot \sqrt{D'} \; ; \; \tilde{i}_s = n \cdot \tilde{i}_p = n \cdot \frac{I_g}{2} \cdot \sqrt{D'} \; ; \; \tilde{i}_D(\mathrm{FW}) = \begin{cases} n \cdot \frac{I_g}{2} \cdot \sqrt{\frac{D'}{2}}, \text{diodes thermally isolated} \\ n \cdot \frac{I_g}{2} \cdot \sqrt{D'}, \text{diodes thermally shorted} \end{cases}$$

$$\Rightarrow \kappa_p = \frac{1}{\sqrt{D'}} \; ; \; \kappa_s = \frac{1}{\sqrt{D'}} \; ; \; \kappa_Q = \sqrt{1 + D'} \; ; \text{[13]}$$

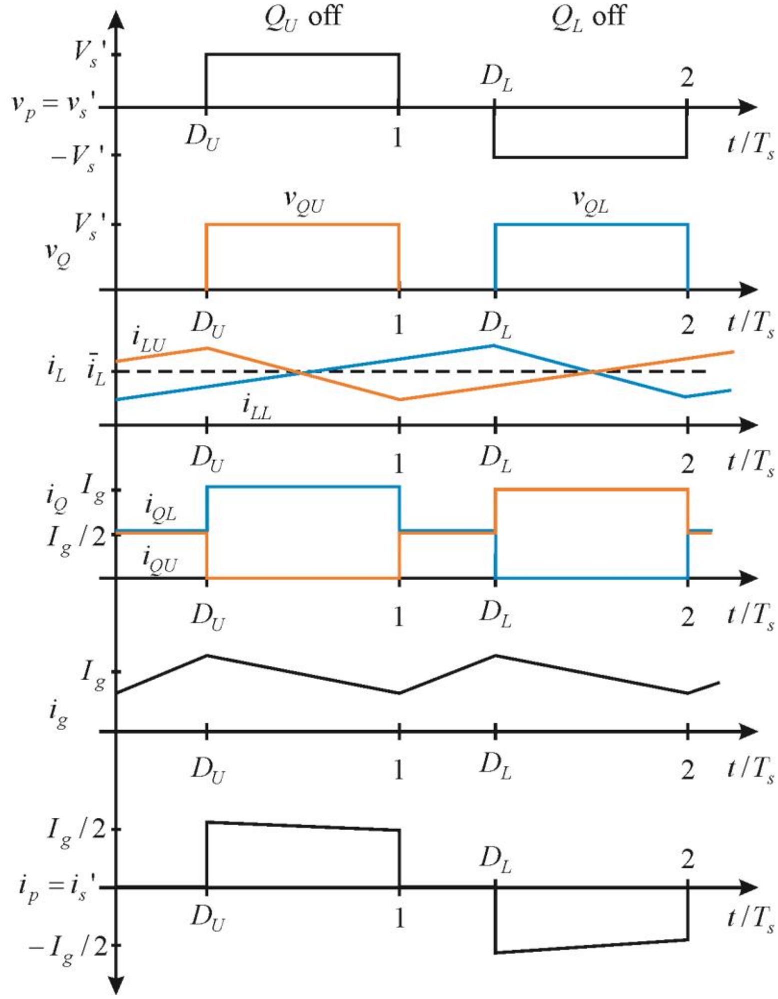

Fig. 4. Differential BPP (DBPP) waveforms. The current waveforms of the two inductors are interleaved, reducing input current ripple. Switch currents i_{QU} and i_{QL} are three-level; during the interval when Q_U is off, i_{QU} = 0 A and i_{QL} = I_g. i_g = i_{QU} + i_{QL} with reduced ripple, though the interleaved inductor currents do not exactly cancel over the D range.

The DBPP voltage ratio from inductor steady-state flux balance, $\Delta\lambda_L$ = 0 V·s, is

$$V_g \cdot (1+D) = (V_s' - V_g) \cdot D' \Rightarrow \frac{V_s'}{V_g} = \frac{2}{D'} \Rightarrow \frac{V_s}{V_g} = \frac{2}{n} \cdot \frac{1}{D'}$$

Unlike the BPP, the form-factor products of the DBPP switches and primary winding are not the same:

$$\kappa_{QD} = \sqrt{\frac{1+D'}{D'}} \text{, diodes thermally shorted (integrated rectifier) ; } \kappa_{ps} = \frac{1}{D'} \Rightarrow \kappa_{CA} = \kappa_{QD} \cdot \kappa_{ps} = \sqrt{\frac{1+D'}{D'^3}}$$

The optimal D minimizes κ_{QD} and κ_{ps} at κ_{QD} = κ_{ps};

$$\sqrt{\frac{1+D'}{D'}} = \frac{1}{D'} \Rightarrow \sqrt{1+D'} = \frac{1}{\sqrt{D'}} \Rightarrow D'^2 + D' - 1 = 0 \Rightarrow D'_{opt} = \frac{\sqrt{5}-1}{2} \approx 0.618 \Rightarrow$$

$$D_{opt} \approx 0.382 \text{ DBPP, BPP}$$

This is the same optimal operating-point as for the BPP as determined in part 11.

The current ripple of the inductors during the on-time interval is

$$\Delta i_L = \frac{V_g \cdot (1+D) \cdot T_s}{L} = (1+D) \cdot \Delta I_{L0}, \; \Delta I_{L0} = \frac{V_g \cdot T_s}{L}$$

During the off-time, inductor current changes (decreases) by

$$-\Delta i_L = \frac{(V_s' - V_g) \cdot D' \cdot T_s}{L} = (2-D') \cdot \Delta I_{L0} = (1+D) \cdot \Delta I_{L0}, \; V_s' = V_g / D'$$

Thus Δi_L(on) and Δi_L(off) have the same magnitude for flux balance. The switch currents average around $I_g/2$ (see third graph above in Fig. 4) and inductor current ripple $i_{LU\sim}(t) \neq -i_{LL\sim}(t)$ around the average i_L. The inductors have equal current ripple amplitude but their currents are interleaved in phase because of their offset by a switching cycle. (They are not *complementary*: one does not respond to D in the same way the other does to D'.)

The inductors have i_L ripple factor

$$\gamma_L = \frac{\Delta i_L / 2}{\bar{i}_L} = \frac{(1+D) \cdot \Delta I_{L0} / 2}{I_g / 2} = 2 \cdot (1+D) \cdot \gamma_{L0}, \; \gamma_{L0} = \frac{\Delta I_{L0} / 2}{I_g}$$

The optimal γ_{opt} of inductor core material matches best to $\gamma_L \approx 0$ of iron-powder.

Δi_L increases linearly with D, but Δi_g depends on the sum of

$$i_g(t) = i_{LU}(t) + i_{LL}(t) \Rightarrow \Delta i_g(t) = \Delta i_{LU}(t) + \Delta i_{LL}(t)$$

During on-time and off-time, i_{LU} and i_{LL} current slope magnitudes are

$$\text{on-time:} \quad m_U = \frac{\Delta i_L}{(1+D) \cdot T_s} = \frac{V_g}{L} \quad \text{(up-slope)}$$

$$\text{off-time:} \quad m_D = \frac{\Delta i_L}{D' \cdot T_s} = \frac{1+D}{D'} \cdot \frac{V_g}{L} = \frac{1+D}{D'} \cdot m_U \quad \text{(down-slope)}$$

The two inductor currents during on-time have the same slope m_U and add; i_g thus has an on-time slope during $D \cdot T_s$ of $2 \cdot m_U$. The slopes are opposed during the off-time; the i_g off-time slope is $-(m_D - m_U)$. The on- and off-time ripple amplitudes of i_g are equal for the above m_U and m_D;

$$2 \cdot m_U \cdot D \cdot T_s = (m_D - m_U) \cdot D' \cdot T_s$$

This results in the total input current ripple;

$$\Delta i_g = 2 \cdot \Delta i_L = 2 \cdot \frac{V_g}{L} \cdot D \cdot T_s = 2 \cdot D \cdot \Delta I_{L0}, \; \Delta I_{L0} = \frac{V_g \cdot T_s}{L}$$

For balance,

$$\frac{V_g}{L_U}\cdot D_U = \frac{V_g}{L_L}\cdot D_L \Rightarrow \frac{D_L}{D_U} = \frac{L_L}{L_U}$$

A tolerance difference between inductor values is corrected by $D_L \neq D_U$ between magnetic half-cycles.

Summary

Compared to the BPP at the same D, V_s/V_g, and transfer power, the DBPP primary winding has half the current ($I_g/2$) at twice the voltage across twice the turns of a BPP primary winding, and is equivalent to a single winding of two BPP windings in series; DBPP n = BPP $2{\cdot}n$. Then in the transfer-ratio of the DBPP, $2/n_{DBPP} = 2/2{\cdot}n_{BPP} = 1/n_{BPP}$ and V_s/V_g is the same for both.

The DBPP off-time switch voltage is the same as the BPP off switches. $\Delta\lambda_p$ and turns both double, keeping both $\Delta\phi_p$ and core loss the same. Field current Ni at half the current and twice the turns as the BPP remains the same, and the transformer γ_{opt} with bipolar magnetizing current i_m continues to match ferrite cores with $\gamma(i_m) = 1$. Transfer-power density is the same in the DBPP and BPP transformers. Overall, the DBPP is a closely competing alternative to the BPP and which one is better will depend on how the above parameters are prioritized in a particular application.

In the next part of the Volksinverter series of articles, we turn attention back to the familiar theme of optimization as we consider the alternative transfer-circuit topology of the CP-BRG (buck, full-bridge) in search of the optimum low-R_g converter. How does the CP-BRG, despite having series switches, compare in performance with the CA-PP (boost push-pull)?

References

1. "Designing An Open-Source Power Inverter (Part 1): Goals And Specifications" by Dennis Feucht, How2Power Today, May 2021.
2. "Designing An Open-Source Power Inverter (Part 2): Waveshape Selection" by Dennis Feucht, How2Power Today, September 2021.
3. "Designing An Open-Source Power Inverter (Part 3): Power-Transfer Circuit Options" by Dennis Feucht, How2Power Today, April 2022.
4. "Designing An Open-Source Power Inverter (Part 4): The Optimal Power-Line Waveshape" by Dennis Feucht, How2Power Today, May 2022.
5. "Designing An Open-Source Power Inverter (Part 5): Kilowatt Inverter Circuit Design" by Dennis Feucht, How2Power Today, July 2022.
6. "Designing An Open-Source Power Inverter (Part 6): Kilowatt Inverter Control Circuits" by Dennis Feucht, How2Power Today, August 2022.
7. "Designing An Open-Source Power Inverter (Part 7): Kilowatt Inverter Magnetics" by Dennis Feucht, How2Power Today, September 2022.
8. "Designing An Open-Source Power Inverter (Part 8): Converter Control Power Supply" by Dennis Feucht, How2Power Today, November 2022.
9. "Designing An Open-Source Power Inverter (Part 9): Magnetics For The Converter Control Power Supply" by Dennis Feucht, How2Power Today, December 2022.
10. "Designing An Open-Source Power Inverter (Part 10): Converter Protection Circuits" by Dennis Feucht, How2Power Today, February 2023.
11. "Designing An Open-Source Power Inverter (Part 11): Minimizing Switch Loss In Low-Input-Resistance Converters" by Dennis Feucht, How2Power Today, March 2023.

12. "Designing An Open-Source Power Inverter (Part 12): Sizing The Converter Magnetics" by Dennis Feucht, How2Power Today, March 2023.

13. "Evaluating Waveform Form Factors Of FW And HW Rectifiers In SMPSs" by Dennis Feucht, How2Power Today, April 2023.

About The Author

Dennis Feucht has been involved in power electronics for 40 years, designing motor-drives and power converters. He has an instrument background from Tektronix, where he designed test and measurement equipment and did research in Tek Labs. He has lately been working on projects in theoretical magnetics and power converter research.

For further reading on inverter design, see the How2Power Design Guide, locate the Power Supply Function category and select "DC-AC power inverters."